ORIGINAL ARTICLE

Zein-based nanocarriers for the oral delivery of insulin. In vivo evaluation in *Caenorhabditis elegans*

Ana L. Martínez-López[1] · Carlos J. González-Navarro[2] · José L. Vizmanos[3,4] · Juan M. Irache[1]

Abstract

The aim was to evaluate the potential of nanocarriers, based on the coating of zein nanoparticles (ZNP) with a Gantrez® AN-PEG conjugate (GP), for the oral delivery of insulin. ZNP-GP displayed less negative surface charge and a 14-fold higher diffusion coefficient in pig intestinal mucus than ZNP. Both nanoparticles showed a spherical shape and an insulin load of 77.5 µg/mg. Under simulated gastric conditions, ZNP-GP released significantly lower amount of insulin than ZNP, while under simulated intestinal conditions, both types of nanoparticles displayed similar behaviour. In *Caenorhabditis elegans* wild-type N2, grown under high glucose conditions, insulin treatments reduced glucose and fat accumulation without altering the growth rate, the worm length, or the pumping rate. The effect was significantly greater ($p < 0.001$) when insulin was nanoencapsulated in ZNP-GP compared with that encapsulated in ZNP or formulated in solution. This would be related to the highest capability of ZNP-GP to diffuse in the dense peritrophic-like layer covering intestinal cells in worms. In *daf-2* mutants, the effect on fat and glucose reduction by insulin treatment was suppressed, indicating a DAF-2 dependent mechanism. In summary, ZNP-GP is a promising platform that may offer new opportunities for the oral delivery of insulin and other therapeutic proteins.

Keywords Nanoparticles · Oral delivery · Mucus-permeating · Zein · PEG · *C. elegans*

Introduction

Peptide-derived drugs have shown a great potential as therapeutics. From the first human recombinant insulin marketed in 1982 [1], to the present, there are more than 68 peptides drugs approved for clinical use by different regulatory agencies [2]. Another 155 candidates are in active clinical development, of which about 50% are in Phase II studies [3]. The global market for peptide drugs has been predicted to increase from US$ 23.3 billion in 2018 to an estimated US$ 49.5 billion in 2027 [4]. The key factor in this success can be attributed to the high target-selectivity of peptide drugs which results in a reduction in undesirable side effects and toxicity [5]. Thus, these biomolecules have become one of the main alternatives for the treatment of more than 150 different pathologies, including cancer, diabetes, autoimmune, and infectious diseases [6]. The vast majority of these therapeutical agents are only available for parenteral administration despite the fact that this form requires sterility and non-pyrogenic conditions, that hinder the manufacturing process, and generates low adherence, particularly among patients who need daily medication to control the disease. In this context, it has been estimated that diabetic patients take more than 60,000 injections in their lifetime, so it seems highly desirable to find alternative routes of administration [7].

From a general point of view, the oral administration offers some advantages (i.e., simplicity, cost-effective, and convenience) that make it the most convenient for a large majority of biologically active compounds. Particularly for diabetic individuals treated with insulin,

✉ Juan M. Irache
 jmirache@unav.es

1 NANO-VAC Research Group, Department of Chemistry and Pharmaceutical Technology, School of Pharmacy and Nutrition, University of Navarra, 31080 Pamplona, Spain

2 Center for Nutrition Research, School of Pharmacy and Nutrition, University of Navarra, 31080 Pamplona, Spain

3 Department of Biochemistry & Genetics, School of Science, University of Navarra, 31080 Pamplona, Spain

4 Navarra Institute for Health Research (IdiSNA), 31080 Pamplona, Spain

this route is very attractive because it can prevent invasive administration and peripheral hyperinsulinemia associated with retinopathies and neuropathies [8, 9]. However, the oral administration of insulin has important limitations, including its enzymatic inactivation in the gastrointestinal tract (GIT) and a poor permeability to pass across the intestinal epithelium [10, 11]. To solve these obstacles and improve its oral bioavailability, the encapsulation in biodegradable nanoparticles may be a valid option [6, 12]. However, in many cases, these nanoparticles have shown a limited efficacy due to their high interaction with mucins and other components of the protective mucus gel layer lining the epithelium that limits their residence time in close contact with the absorptive membrane. In fact, the mucus barrier is a complex and viscous hydrogel that is continuously produced, secreted, and finally removed. It acts as a natural barrier against the free diffusion of macromolecules and other microscopic components (including nanoparticles), hindering their arrival at the epithelium [10].

One strategy to minimize these interactions would be the modification of the surface of nanoparticles with hydrophilic compounds that confer a "slippery" corona that would enhance the diffusion of the nanoparticles in the deeper mucosal regions and facilitate their arrival at the surface of the cells that constitute the gut epithelium (i.e., enterocytes). Based on this approach, mucus-permeating nanocarriers have been produced by the coating of nanoparticles with poly(ethylene glycol)s [13, 14] or Pluronic®F 127 [15].

The aim of this work was to evaluate the potential and capabilities of zein-based nanoparticles as carriers for the oral delivery of insulin. Zein is a Generally Recognised as Safe (GRAS) material that can yield nanoparticles by simple procedures and with a significant ability to load biomacromolecules without compromising their integrity and activity [16]. However, zein nanoparticles have important mucoadhesive properties [17, 18] that limit their capability to reach the absorptive epithelium.

To minimize this inconvenience, in this work, zein nanoparticles were coated with a hydrophilic polymer conjugate obtained by the covalent binding of PEG 2000 to Gantrez® AN. Nanoparticles from this polymer conjugate have demonstrated their ability to increase the bioavailability of drugs with low permeability (i.e., docetaxel [19]). However, both the use of organic solvents during the preparation of these nanoparticles and the reactivity of the polymer conjugate with functional groups of proteins is detrimental to the activity of insulin. To solve these problems, in this case, insulin was encapsulated in zein nanoparticles containing a hydrophilic corona of a Gantrez AN-PEG polymer conjugate. Finally, the resulting nanocarriers were evaluated in *C. elegans* as an in vivo model.

Materials and methods

Materials

Poly(ethylene glycol) 2000 (PEG) was provided by Fluka (Buchs, Switzerland). Gantrez® AN 119 or poly(anhydride) (MW of 97.7 kDa) was a gift from Ashland Inc. (Covington, KY). Zein, lysine, human insulin, Nile red, Orlistat, glucose, isopropanol, sodium azide, tripton X-100, agarose, mannitol, and Rose Bengal salt were purchased from Sigma-Aldrich (St Louis, MO). Lumogen®F Red was provided by BASF (Ludwigshafen, Germany). Acetone and ethanol were obtained from Scharlab (Sentmenat, Spain). Dichloromethane was supplied by Merck (Darmastadt, Germany).

Preparation of Gantrez® AN-PEG2000 conjugate

The conjugate was obtained by the covalent binding of PEG2000 to the poly(anhydride) groups of Gantrez® AN following a procedure previously described [19], with some minor modifications. Briefly, a solution of PEG2000 in acetone was added by dripping in a second solution of Gantrez® AN in the same solvent. The mixture was heated to 50 °C, with moderate stirring for 3 h. Then, the solvent was eliminated under reduced pressure in a Büchi R-144 apparatus (BÜCHI Labortechnik AG, Flawil, Switzerland) until the conjugate was completely dry. The remaining powder was collected and washed with dichloromethane (to eliminate the remaining free PEG) before filtration under vacuum (all-glass filter, Merck Millipore, Darmstadt, Germany). Finally, the resulting powder was stored in dry conditions. The conjugate was named GP.

The GP conjugate was confirmed and characterized by ^{1}H-NMR and FT-IR and showed a degree of substitution of 7.4% and MW of 103.11 kDa.

Preparation of nanoparticles

Zein nanoparticles, containing insulin, were prepared by a desolvation procedure previously described [17, 18], coated by simple incubation with the GP conjugate and, after purification, dried in a Spray-drier apparatus.

In brief, 200 mg zein, 30 mg lysine, and 20 mg insulin were dissolved in 20 mL of a mixture of ethanol and water (55:45 by vol.). The nanoparticles were obtained by adding 20 mL purified water under shaking. Then, 0.5 mL of a GP conjugate solution in water (2.5% w/v) was incorporated and the mixture was kept stirred for 30 min. The suspension was purified and concentrated by ultrafiltration and, after the addition of mannitol as protectant, dried in a Büchi Mini

Spray Drier B-290 (Büchi Labortechnik AG). The insulin-loaded nanoparticles were named I-GP-ZNP.

The uncoated nanoparticles (I-ZNP) were prepared in the same way but in the absence of the GP conjugate. Similarly, empty nanoparticles were also prepared but in the absence of insulin (GP-ZNP and ZNP respectively).

Furthermore, the nanoparticles were fluorescently labelled with Lumogen®F Red 305. For this, 5 mg Lumogen® F Red were dissolved in the hydroalcoholic solution of zein before the nanoparticles were formed. The nanoparticles were obtained and dried as described above.

Characterization of nanoparticles

Particle size, zeta potential, and yield

The particle size, polydispersity index (PDI), and zeta potential of nanoparticles were determined by photon correlation spectroscopy (PCS) and electrophoretic laser Doppler anemometry respectively, using a Zetasizer analyser system (Brookhaven Instruments Corp., Holtsville, NY). The diameter of the nanoparticles was determined after dispersion in ultrapure water, whereas the zeta potential was determined in a 0.01 mM KCl solution adjusted to pH 7.4.

The amount of protein transformed into nanoparticles was quantified by electrophoresis. For this, 5 mg of each formulation were dispersed in water and centrifuged at $15,000 \times g$ for 20 min. Supernatants were discarded, and the pellets were dissolved in ethanol 75% before analysis in a capillary electrophoresis-Experion system (Bio-Rad Laboratories, Hercules, CA). For data analysis, Experion software version 3.10 (Bio-Rad Laboratories) was used. The amount of protein forming nanoparticles in the formulation was estimated as the ratio, expressed as a percentage, between the amount of the zein quantified in the pellet of the centrifuged samples and the total amount of zein used for the preparation of nanoparticles.

Morphology and Shape

The shape and surface morphology of the nanoparticles were examined by SEM. Briefly spray-dried nanoparticles were dispersed in water and centrifuged at $28,000 \times g$ for 20 min to remove the mannitol. The pellet was re-dispersed in water and mounted on SEM grids, dried, and coated with a gold layer using a Quorum Technologies Q150R S sputter-coated (Ontario, Canada) and analysed using a ULTRA plus ZEISS field emission scanning electron microscope (FEG-SEM Zeiss Sigma 500, Jena, Germany). SEM images were obtained in secondary and backscattered electron imaging mode.

Quantification of insulin

The insulin loading was determined by HPLC as previously described [18] in an Agilent model 1100 series (Agilent Technologies, Waldbronn, Germany), coupled with photodiode array detection system set at 220 nm. A TSKgel4000 column (7.8 mm × 30 cm; Tosoh Bioscience GmbH, Griesheim, Germany) was used as stationary phase, whereas the mobile phase was a 0.3-M NaCl solution in 0.05-M phosphate buffer at a flow-rate of 0.8 mL/min. Standard curves in the range of 2–100 μg/mL ($R^2 \geq 0.999$) were prepared, and the samples were assayed in triplicate.

For analysis, nanoparticles, dispersed in water, were centrifuged and the pellet dissolved in ethanol 70% prior analysis. The payload was expressed as the amount of insulin (in microgram) per milligram of nanoparticles. The encapsulation efficiency (EE, expressed in percentage) was calculated as the quotient between the amount of insulin quantified in the pellets and the amount initially added for the preparation of nanoparticles.

Quantification of Lumogen® F red 305

Lumogen® F Red 305 red was quantified by UV-Vis spectrometry at 580 nm (Labsystems iEMS Reader MF, Vantaa, Finland) by difference between the initial amount of fluorescent dye incorporated in the nanoparticles and the amount quantified after digesting the nanoparticles with 75% ethanol. Standard curves were constructed in 75% ethanol (concentration range of 5–30 μg/mL; $R^2 \geq 0.999$).

Surface hydrophobicity evaluation

The surface hydrophobicity of the different nanoparticles was estimated by the Rose Bengal method [20]. Briefly, 500 μL of nanoparticle dispersions in water (from 0.04 to 4 mg/mL) were mixed with 1 mL of an aqueous solution of Rose Bengal (100 μg/mL). The samples were incubated for 30 min at 25 °C with constant shaking at 1500 rpm and, then, centrifuged at $13,500 \times g$ for 30 min in a MIKRO 220 centrifuge (Hettich, Tuttlingen, Germany). The amount of Rose Bengal in the supernatants (unbound Rose Bengal) was calculated by measuring the absorbance at 548 nm, using a microplate reader (BioTek PowerWave XS, BioTek Instruments Inc., Winooski, VT).

For calculations, the total surface area (TSA) of nanoparticles (calculated using Eq. 1) was determined by assuming that the nanoparticles were spherical in shape and monodisperse, with a diameter equal to the mean size determined by DLS.

$$\text{TSA} = (\text{SA}_{NP}) \text{ x } (\text{NT}_{NP}) \tag{1}$$

where SA_{NP} is the surface of one individual nanoparticle ($4\pi r^2$) and NT_{NP} is the total number of nanoparticles in each dilution, calculated using the Eq. 2:

$$NT_{NP} = m_{NP}/(\rho zein \ X \ V_{NP}) \tag{2}$$

where m_{NP} is the weight of the nanoparticles in each dilution, $\rho zein$ is the density of zein (1.41 g/mL calculated by pycnometry), and V_{NP} is the volume ($4/3\pi r^3$) of an individual nanoparticle.

On the other hand, the partitioning quotient (PQ) was calculated as the quotient between the amount of the Rose Bengal bound and unbound. Plotting of PQ against TSA of nanoparticles resulted in straight lines. The slope of the line of the chart represents the hydrophobicity of the formulation. The higher the slope, the higher the hydrophobicity.

Ex vivo mucus diffusion studies in pig intestinal mucus

Collection and preparation of porcine mucus

Porcine mucus was obtained from small intestines collected from the slaughterhouse. For this, intestines were cut in small portions that were opened to expose the lumen. The exposed lumen was cleaned with PBS, and the mucus was collected with a spatula, avoiding drag of epithelial tissue. The mucus was transferred to vials and stored at -80 °C.

Multiple particle tracking in mucus

Diffusion of nanoparticles through intestinal mucus was evaluated using the MPT technique, previously described [21, 22]. Briefly, samples (0.5 g) of pig intestinal mucus were incubated in glass-bottom MatTek imaging dishes (MatTek Corp., Ashland, MA) at 37 °C. Then, a 25-μL aliquot of a suspension of fluorescently labelled nanoparticles (0.002%) was added and gentle shaking for 2 h (for efficient distribution of nanoparticles) before the video recording. Videos of 10 s at 30 frames/s were captured on a Leica DM IRB wide-field epifluorescence microscope ($\times$ 63 magnification oil immersion lens, Leica Camera AG, Wetzlar, Germany) using a high-speed camera (Allied Vision Technologies, Stadtroda, Germany). At least 100 individual trajectories from each sample were tracked and analysed. The MPT of each formulation was carried out in triplicate.

The videos were analysed using the Fiji ImageJ software [23]. The trajectory of each nanoparticle was then converted to numeric pixel data and, finally, to metric distances (based on the recording settings). The displacement of each nanoparticle over time was expressed as squared displacement (SD). The mean square displacement (MSD)

was calculated as the geometric mean of the SD of the nanoparticle along its entire trajectory as

$$MSD = (X\Delta t)^2 + (Y\Delta t)^2 \tag{3}$$

Then, the effective diffusion coefficient (D_{eff}) of each formulation was calculated using the following formula:

$$D_{eff} = <MSD> /(4x\Delta t) \tag{4}$$

where 4 is a constant relating to the 2-dimensional mode of video capturing and Δt is the selected time interval.

In parallel, the diffusion of the nanoparticles in water ($D°$) was calculated by the Stokes–Einstein equation at 37 °C:

$$D° = kT6\pi\eta r \tag{5}$$

In which "k" is the Boltzmann constant, T is absolute temperature, η is water viscosity, and "r" is the mean radius of nanoparticles.

In vitro release studies

Release studies were performed in simulated gastric (SGF; pH 1.2) and intestinal (SIF; pH 6.8) fluids. Drug-release patterns were evaluated by using Float-A-Lyzer® devices with a MWCO of 300 kDa (Spectrum Labs, Breda, The Netherlands). The dialysis bags were filled with a suspension of nanoparticles in water (containing 10 mg insulin) and placed in 45 mL SGF at 37 °C with magnetic shaking. After 2 h of incubation in SGF, the bags were transferred to a second vessel with 45 mL of SIF. At fixed time intervals, 500-μL samples were drawn and replaced with equal volumes of fresh simulated fluid to maintain a constant release volume. Insulin was quantified by the HPLC method described above. Calibration curves in the simulated media (2–100 μg/mL; $R^2 \geq 0.999$ in both cases) were performed, and release profiles were expressed in terms of cumulative release percentage, and plotted versus time.

In vivo evaluation of nanoparticles using *C. elegans*

Strains and cultivation

C. elegans wild-type N2 Bristol and *daf-2*(e1370) III (CB1730) mutant strains was obtained from Caenorhabditis Genetics Center (CGC, University of Minnesota). Living *Escherichia coli* (OP50) was used as normal nematode diet. All strains were maintained at 20 °C on Nematode Growth Medium (NGM) agar plates as described previously [24].

Treatment with nanoparticles

The assays were performed in triplicate in 6-well cell culture plates with 4 mL of glucose-supplemented (50 mM) NGM

per well. Orlistat (6 μg/mL) was used as a positive control of fat reduction in *C. elegans*. The effect of insulin (dissolved in water or encapsulated in nanoparticles) on *C. elegans* was evaluated at a concentration of 50 IU/mL in NGM. Negative controls were prepared by adding the same amount of water to plates.

For all experiments, age-synchronized worms (either wild-type N2 or *daf-2* mutant) were obtained by hypochlorite treatment (in which only eggs can survive), and the eggs were let hatch overnight in M9 buffer solution. Then, approximately 500 L1 larvae were transferred to plates and grown until the L4 stage.

Fat content quantification

The quantification of the fat content in the nematodes was performed by the fixative-based Nile Red method [25]. For this, L4 worms were harvested and washed with PBST and fixed in 40% isopropanol. Staining was performed by adding a fresh Nile Red solution (3 μg/mL). After that, the worms were washed again in PBST and mounted on a 2% agarose pad for microscopy evaluation. Fluorescent images of Nile Red-stained worms were captured at × 80 magnification on a Nikon SMZ18 stereomicroscope (Nikon Instruments Inc., Tokyo, Japan) equipped with an epifluorescence system and a DS-Fi1C refrigerated colour digital camera (Nikon). Images were taken under a GFP filter (Ex 480–500, DM 505; BA 535–550) and analysed using ImageJ software.

Measurement of pumping rate, growth rate and worm size

All these physiological parameters were analysed in N2 wild-type *C. elegans*. After the 48 h treatment, the nematodes were transferred to new plates with fresh *E. coli* OP50. For pumping rate quantification, the number of pharyngeal muscle contractions of 12 randomly selected worms was counted for 1 min in Nikon SMZ18 stereomicroscope (Nikon Instruments Inc., Tokyo, Japan) [26]. The growth rate was

determined by counting the number of worms at different stages under an optical microscope. For this purpose, 50 worms each treatment were randomly selected and paralysed using 10 mM NaN$_3$ [27]. For body size measurement, a 30-s video was recorded and used to measure the length and width of worms using the Wormlab tracking system (WormLab software, MicroBrightField Inc., Williston, VT).

Statistical analysis

Means and standard errors were calculated for each data set. The reduction in body fat between treatments was evaluated using a hierarchical ANOVA followed by multiple comparison (Fisher's, LSD) tests. For the rest of the parameters, statistical analyses were performed using a one-way ANOVA followed by a Tukey-Kramer multi-comparison test. All calculations were performed using Stata/SE v12 software (Stata Corp, LLC, College Station, TX), and the curves were plotted with Origin 8 software (OriginLab Corp, Northampton, MA).

Results and discussion

Characterization of nanoparticles

The main physicochemical properties of insulin-loaded nanoparticles are summarized in Table 1. The average diameter was affected by the incorporation of insulin into nanoparticles; the insulin-loaded nanoparticles displayed a larger size with an increase of ca. 9–10% compared with the empty nanoparticles. Meanwhile, the coating with GP conjugate significantly decreased the negative zeta potential of the nanoparticles (from − 45 to − 38 mV; $p < 0.01$). This result agrees with previous studies in which it was shown that covering nanoparticles with PEG-containing copolymers resulted in a higher zeta potential [14, 28]. In any case, the PDI values of

Table 1 Physicochemical properties of empty (ZNP and GP-ZNP) and insulin-loaded zein nanoparticles (I-ZNP and I-GP-ZNP) and ratios of their ensemble average diffusion coefficients in mucus (D_m) and in water (D_w)

	ZNP	I-ZNP	ZNP-GP	I-ZNP-GP
Size (nm)	209 ± 5	231 ± 8	227 ± 4	248 ± 9
PDI	0.11 ± 0.01	0.14 ± 0.08	0.10 ± 0.06	0.12 ± 0.08
Zeta potential (mV)	− 45 ± 1	− 42 ± 2	− 39 ± 1	− 38 ± 2
Yield (%)	82 ± 3	81 ± 2	84 ± 5	82 ± 3
D_m/D_w+	7000	nd	500	nd
Insulin loading (μg/mg NP)	-	75.3 ± 2.68	-	77.5 ± 2.01
EE (%)	-	86.8 ± 1.23	-	88.7 ± 2.43

Data are expressed as mean ± S.D.; $n \geq 3$ *nd* not determined

+D_m values are obtained at a time scale of 1, and D_w is calculated from the Stokes-Einstein equation

all nanoparticles were lower than 0.15, which implies monodisperse formulations. Likewise, the yield of the preparative process was quite similar and around 84%.

The morphology of nanoparticles by SEM is shown in Fig. 1. Both types of nanoparticles (uncoated and GP-coated) displayed a spherical shape, but with apparent differences in their surface. Uncoated nanoparticles showed a clearly smooth surface, while GP-ZNP displayed a rough surface, probably due to the presence of the GP conjugate on the surface of nanoparticles. In addition, GP-coated nanoparticles appeared to be slightly higher than uncoated ones, which was consistent with spectroscopy results (Table 1). On the other hand, the surface hydrophobicity of nanoparticles was evaluated by comparing the adsorption to the nanoparticles of Rose Bengal. Data are plotted as total surface area

(TSA) versus partition quotient, where the increase in slope is proportional to the increase in hydrophobicity of the nanoparticles (Fig. 2). GP-coated nanoparticles were significantly less hydrophobic and displayed a 1.6-fold lower slope than bare nanoparticles ($p < 0.01$). This finding, as well as the reduction of the surface negative charges of GP-ZNP, evidenced the presence of the conjugate on the surface of zein nanoparticles.

The insulin loading in zein nanoparticles was calculated to be close to 77 µg/mg nanoparticles, with encapsulation efficiencies of approximately 87% (Table 1). Interestingly, the coating of zein nanoparticles with GP did not affect the insulin payload. For fluorescence-labelled nanoparticles, the amount of Lumogen® F Red 305 incorporated into the nanoparticles was 0.73 ± 0.05 µg/mg.

Nanoparticle transport in pig intestinal mucus ex vivo

The influence of the GP coating on the diffusion of nanoparticles through porcine intestinal mucus was evaluated by multiple particles tracking (MPT). The trajectories of particles were converted into geometric ensemble mean-squared displacements ($<MSD>$) as a function of time. As shown in Fig. 3a, the GT-coated nanoparticles significantly increased their transport rates ($p < 0.01$). In fact, $<MSD>$ of PG-NPZ was 14-times higher than for bare nanoparticles. On a 1 s time scale, the average effective diffusivity ($<D_{eff}>$) of GP-ZNP was only 500-fold lower than their theoretical speed in water, while that of bare
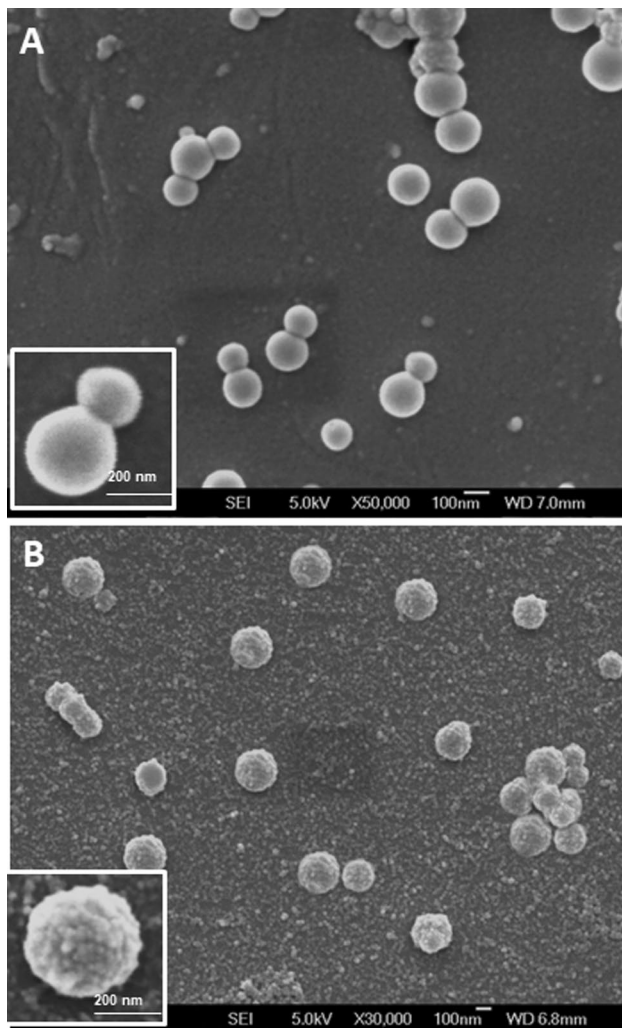

Fig. 1 Scanning electron microscopy (SEM) images of spray-dried nanoparticles. **a** Uncoated nanoparticles (ZNP); **b** GP-coated nanoparticles (GP-ZNP). A magnification of a section of each micrograph is shown in the lower left
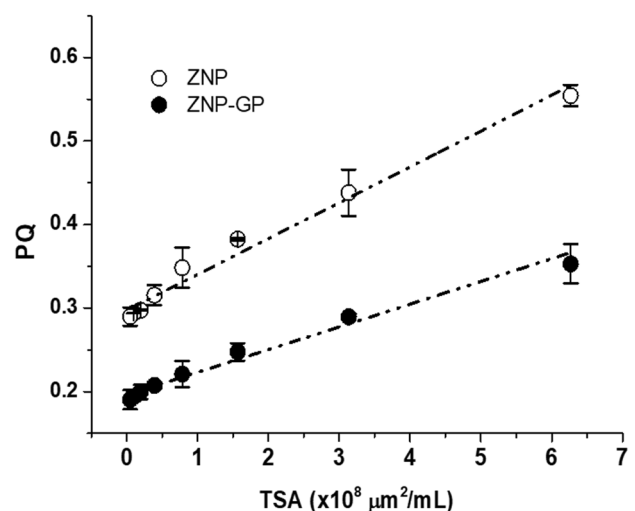

Fig. 2 Relative hydrophobicity as measured by Rose Bengal adsorption on the surface of nanoparticles. Partition quotient (PQ) *vs* total surface area (TSA) of bare (I-ZNP) and GP-coated nanoparticles (I-ZNP-GP). The dotted lines represent the linear regression where the slopes are proportional to the relative hydrophobicity of the nanoparticles. Data are presented as mean ± S.D ($n = 3$)
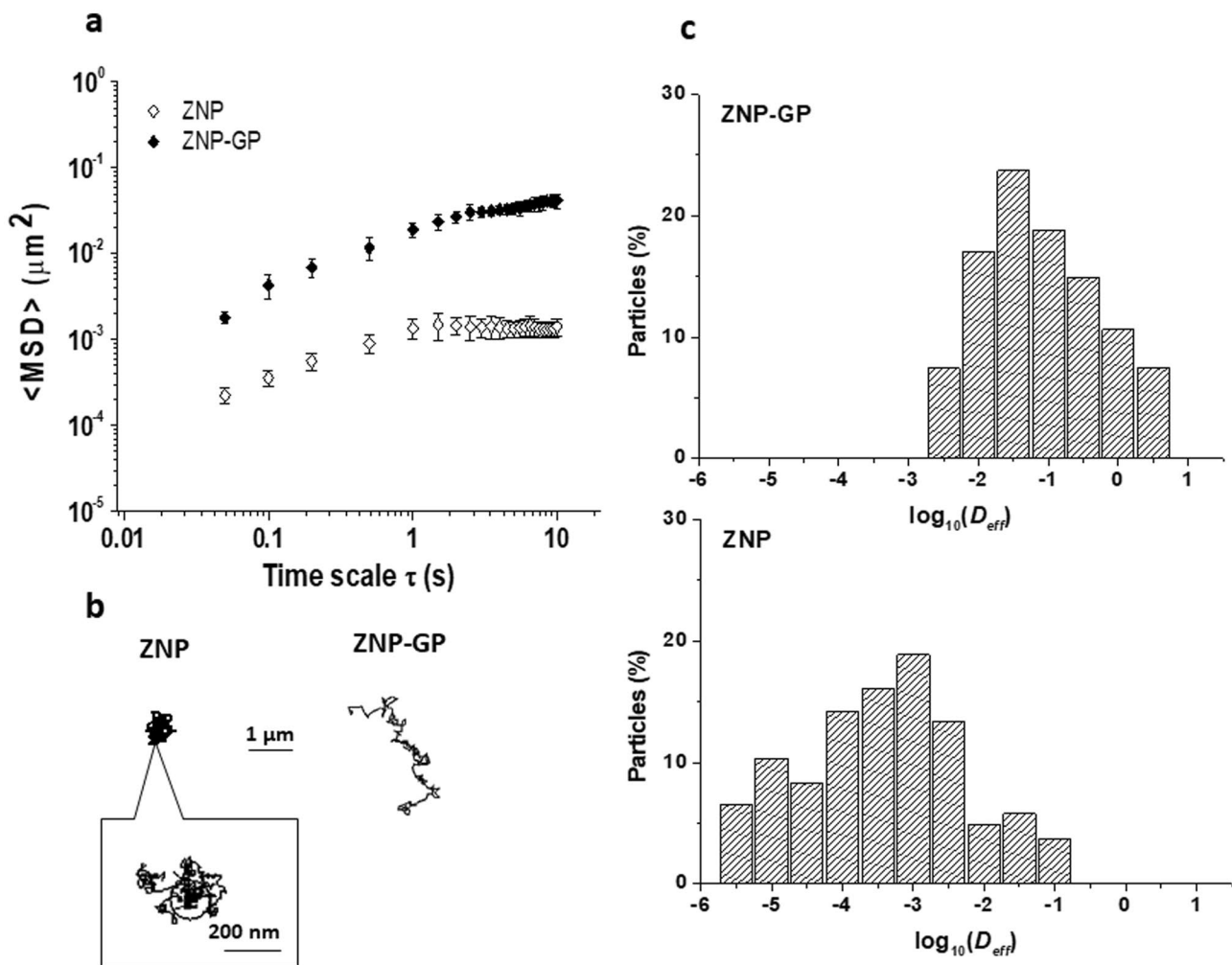
Fig. 3 Transport of uncoated and GP-coated zein nanoparticles in pig intestinal mucus. **a** Ensemble-averaged geometric mean-squared displacements (<*MSD*>) as a function of time scale. **b** Representative trajectories of uncoated (ZNP) and GP-coated zein nanoparticles (GP-ZNP), with effective diffusivities within one S.E.M. at a time scale of 1 s. **c** Distribution of the logarithms of individual particle effective diffusivities (D_{eff}) at a time scale of 1 s. Data represents three independent experiments, with $n \geq 100$ particles for each experiment

nanoparticles was more than 7,000-fold lower (Table 1). This difference in the transport rates of nanoparticles was also reflected by the slope α of double logarithmic *MSD vs* time scale plot ($α = 1$ for free diffusion; $α < 1$ reflects increased obstruction to particle movement). The average α for PG-ZNP and ZNP was 0.80 and 0.34, respectively.

The representative trajectories of the movement of nanoparticles in mucus further emphasize these differences in transport behaviour (Fig. 3b), since the movement of GP-ZNP reflected Brownian-type trajectories that explored distances much wider than their diameters. In contrast, the trajectories of ZNP were highly restricted, non-Brownian time-lapse traces of the particles in the mucus.

To confirm that the observed average transport rate of GP-ZNP was not influenced by a small fraction of outlier fast-moving nanoparticles, we evaluated the distribution of

individual particle by measuring the effective diffusivity (D_{eff}) over a time interval of 1 s. The logarithmic D_{eff} distributions showed that the average mobility of GP-ZNP was due to a near-uniform increase in individual particle velocities compared with uncoated ZNP (Fig. 3c). Thus, coating zein nanoparticles with the GP conjugate not only reduced the obstruction to the movement of the particles but also increased the homogeneity of the transport of such nanoparticles.

Both types of the nanoparticles evaluated in this work, GP-ZNP and ZNP, displayed mean sizes similar to the average mesh size of the mucin network in pig intestinal mucus (estimated average 210 nm, with 90% falling between 100 and 300 nm [29]). Consequently, the improved mobility of GP-ZNP compared with ZNP may be attributed to the hydrophilic shield provided by

GT on the surface of the nanoparticles, which would be effective in minimizing the interactions of the zein nanoparticles with the mucins and, thus, their trapping in the mucus network. These results agree with previous studies showing that the "decoration" of nanoparticles with PEG would reduce the interactions of the particle surface with the hydrophobic domains or glycosides bonds of mucin fibres [14, 30]. Therefore, it is possible to hypothesize that the hydrophilic moieties of PEG would be mainly oriented towards the outside, forming a hydrophilic corona-type surface, which would confer a muco-inert effect on the resulting nanoparticles.

In vitro release studies

Figure 4 shows the insulin release profile from I-ZNP and I-ZNP-GP formulations when incubated in simulated gastric fluid (SGF), for 2 h, followed by incubation in simulated intestinal fluid (SIF). In SGF, I-ZNP-GP released about 28% of their insulin content in 2 h. This amount of insulin was significantly less than that released from I-ZNP (about 50% in 2 h; $p < 0.05$). This indicates that the GP coating layer would act as a barrier against insulin diffusion and decreased its release rate in SGF. When the nanoparticles were transferred to SIF, insulin continued to be released at a slightly lower rate for both formulations, with no remarkable differences between both formulations. At the end of the experiment, the total amount of insulin released from GP-coated and bare nanoparticles was about 84% and 97%, respectively.
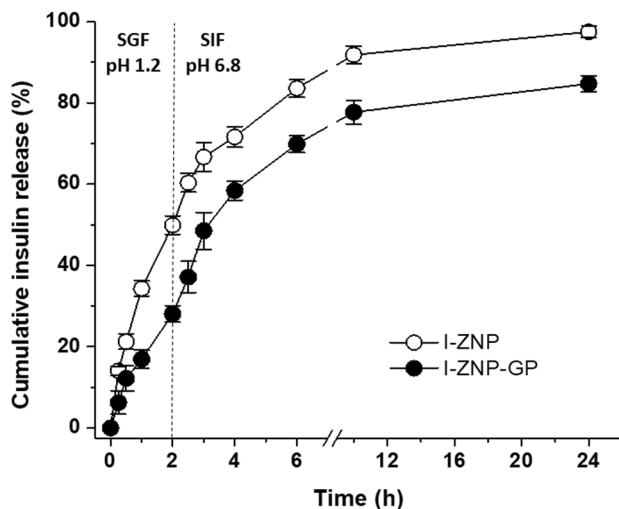

Fig. 4 In vitro insulin release profile from bare (I-ZNP) and GP-coated nanoparticles (I-ZNP-GP) in simulated gastric fluid (SGF) and simulated intestinal fluid (SIF) at 37 °C. Data are represented as mean ± S.D. ($n = 3$)

In vivo evaluation of insulin-loaded nanoparticles in *C. elegans*

Insulin/IGF-1 signalling (IIS) pathway is highly conserved between *Caenorhabditis elegans* and humans. The *C. elegans* IIS pathway connects nutrient levels to metabolism, growth, development, behaviour, and longevity. *C. elegans* DAF-2 is a transmembrane receptor homolog of the human insulin/IGF receptor. The activation of DAF-2/IIS pathway by a high-glucose diet in *C. elegans* has been shown to cause toxicity, which results in an increase of lipogenesis and a decrease in lifespan [31, 32]. Thereby, the efficacy of insulin-loaded nanoparticles in *C. elegans* under high glucose conditions was evaluated, comparable with the blood glucose levels observed in diabetic patients [33–35]. For this purpose, N2 wild-type worms and *daf-2* mutant (loss-of-function) in larval L4 stage were treated with insulin (formulated in ZNP or GP-ZNP) under high glucose conditions and the fat content was evaluated after 48 h of treatment.

In *C. elegans*, fat is mainly stored in hypodermic and intestinal cells. This fat can be easily detected by staining with lipid affinity dyes such as Nile Red, Oil Red O, and quantified through the transparent body by measuring the intensity of the accumulated dyes [25, 36]. In this study, the fat content of the worms was determined by Nile Red, and Orlistat was used as a positive control of fat reduction (Fig. 5a). Consistent with previous reports, we found that glucose supplementation induced a significant increase in fat accumulation in worms in both, wild-type N2 (about 60%; [37]) and the *daf-2* mutants (about 30%; [38]). In wild-type N2 animals, the treatment with I-ZNP-GP induced a significant reduction in worm fat by 33% ($p < 0.001$), while I-ZNP and free insulin only reduced them by 22 and 14%, respectively ($p < 0.01$) (Fig. 5a and b). This effect on fat storage might be associated with the reduction of intracellular levels of glucose in worms. Thus, the nematodes treated with nanoencapsulated insulin showed a significantly lower glucose content (around 40%, $p < 0.01$) than the worms treated with free insulin (32%, $p < 0.05$) (Fig. 6a). In contrast, with the results observed in wild-type N2, the glucose content (Fig. 6b) and fat accumulation (Fig. 5c) in the *daf-2* mutant were not affected by the insulin treatments. These data suggest that insulin suppresses *daf-2*-mediated pathway-dependent fat accumulation. These results are consistent with a previous study that demonstrated that human insulin induced a reduction of glucose concentration in worms by restoring the activity of glyoxalase-1 activity, which is mediated by a DAF-2/insulin receptor [39].

The effect of insulin on fat accumulation increased when it was encapsulated in nanoparticles. This could be associated with the protection of insulin against enzymatic degradation in the intestine of worms, where several digestive enzymes, mainly proteases, are secreted [40]. In fact, treatment with I-ZNP-GP showed a greater effect in reducing fat content than treatment with bare nanoparticles (Fig. 5a). This observation would be related

Fig. 5 Effect of insulin (free or nanoencapsulated in ZNP or GP-ZNP) on fat accumulation in *C. elegans* grown under high glucose (50 mM) conditions. **a** Fluorescence images after Nile Red staining of N2 worms at L4 stage. Data show the percentage of the fluorescence intensity of **b** wild-type N2 strain and **c** *daf-2* mutant referenced to the fluorescence shown by control (100%). Grey dots represent individual data for *n* ≥ 110 worms from three independent experiments for each strain. The horizontal lines are the mean values in each group, and the vertical lines represent the standard deviation (S.D.). ***$p < 0.001$ for the indicated comparison. ORL Orlistat, I-ZNP insulin-loaded uncoated nanoparticles, I-ZNP-GP insulin-loaded GP-coated nanoparticles
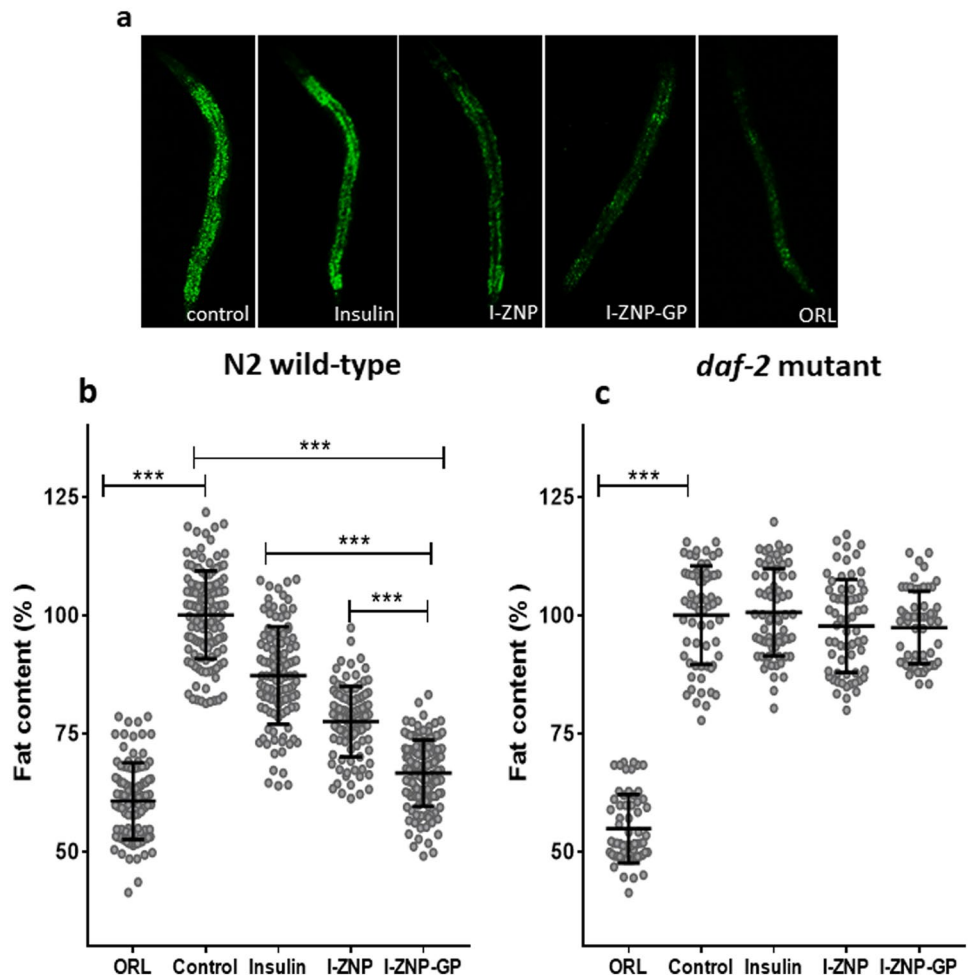
to the higher capability of GP-coated nanoparticles to diffuse in the mucus. The intestinal epithelium of *C. elegans* is protected by a dense peritrophic-like layer, similar to the mucus layer in the human intestinal cells [41].

On the other hand, we also evaluated whether the insulin-loaded nanoparticles had any effects on some physiological parameters of wild-type nematodes, such as worm size, growth rate, and pumping rate. Pumping rate is a mechanical movement, which represents food intake in *C. elegans* [26]. Treatment

Fig. 6 Effects of insulin (free or nanoencapsulated in ZNP or GP-ZNP) on the glucose levels within **a** wild-type N2 strain and **b** *daf-2* mutant grown under high glucose (50 mM) conditions. Data represents three independent experiments with *n* = 50 worms for each experiment. ***$p < 0.001$ for the indicated comparison. I-ZNP insulin-loaded nanoparticles, I-ZNP-GP insulin-loaded GP-coated nanoparticles
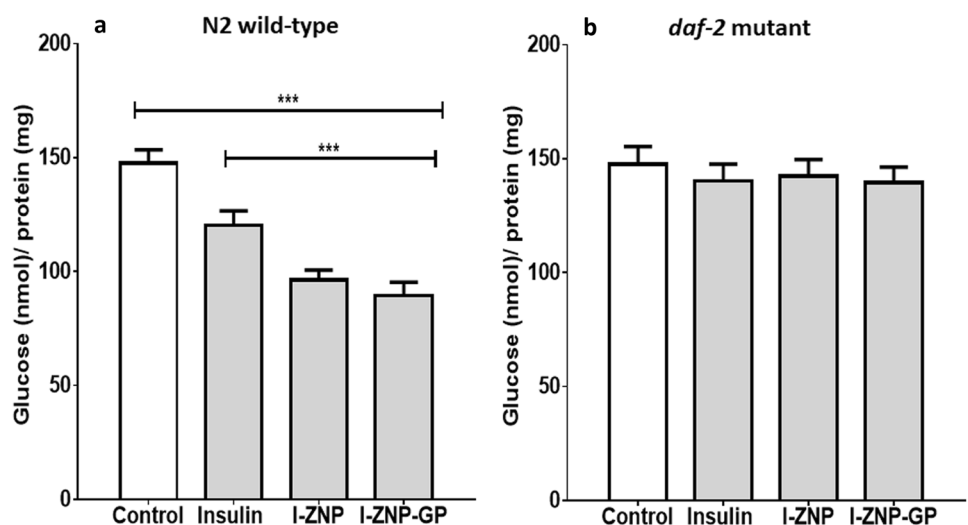
Fig. 7 Effects of insulin (free or nanoencapsulated in ZNP or GP-ZNP) on the growth rate and physiological behaviour in wild type N2 *C. elegans* after the 48 h treatment. **a** Pumping rate: the number of pharyngeal contractions of 12 randomly selected worms. **b** Growth rate: percentage of worms from L1 to adult between treatment and control groups. **c** Worm length: average body length of N2 worms. **d** Worm width: average body width of N2 worms. Data represents means ± S.D. of three independent experiments with $n = 100$ worms for each experiment. *$p < 0.05$ for the indicated comparison. I-ZNP insulin-loaded uncoated nanoparticles, I-ZNP-GP insulin-loaded GP-coated nanoparticles
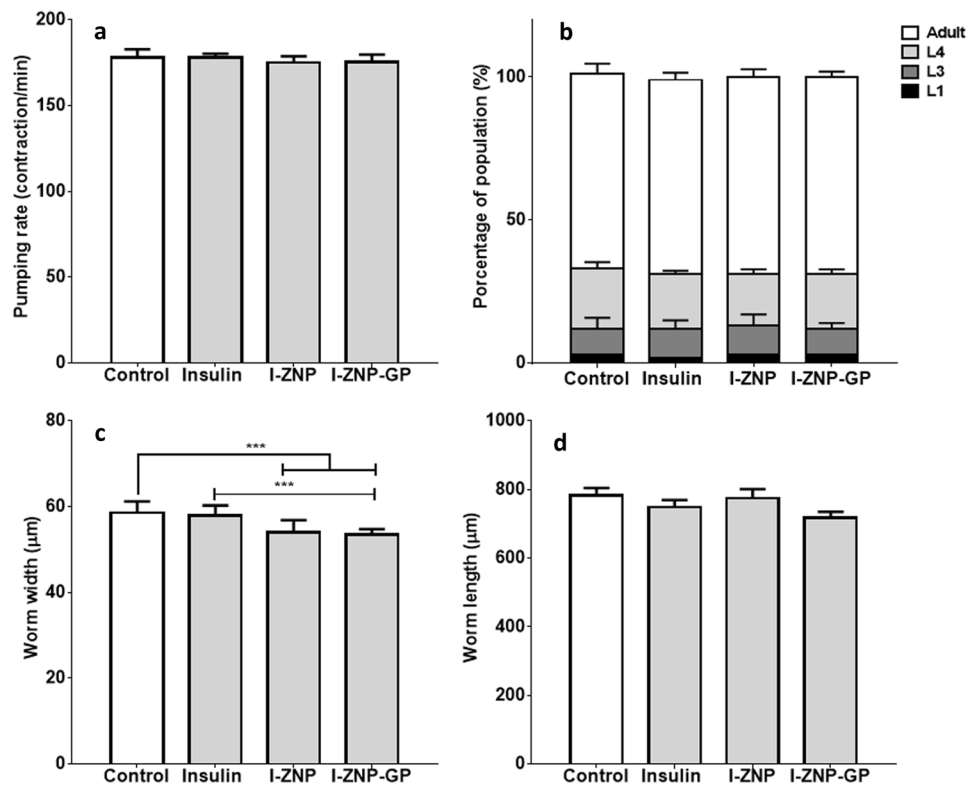
with insulin, both free and encapsulated, for 48 h did not affect the pumping rate of wild type nematodes compared with the controls (Fig. 7a). This suggests that there were no changes in food intake due to the treatments with nanoparticles. The treatments also did not show a significant effect on growth rate (Fig. 7b) and body length (Fig. 7c). The slight reduction in the body width of the worms compared with the control (Fig. 7d) could be due to the reduction in fat accumulation caused by the insulin treatments (Fig. 5a and b).

Taken together, our findings suggest that the encapsulation of insulin in GP-coated nanoparticles promotes the absorption and, thus, the interaction of the protein with its specific receptor (DAF-2/insulin); without altering other physiological properties (worm length, growth rate and pumping rate).

Conclusion

In summary, zein-based nanoparticles, coated with a polymer conjugate of Gantrez®AN and PEG, improved diffusion in intestinal mucus, transforming the mucoadhesive nanoparticles into mucus-permeating ones. In the *C. elegans* model, these insulin-loaded nanoparticles (I-ZNP-GP) induced a significant reduction in the glucose content and fat accumulated in the body, without altering other physiological properties (worm length, growth rate and pumping rate). Furthermore, in high glucose-fed *daf-2* mutants, the lack of effect on fat reduction by insulin

treatment is indicative of a DAF-2 dependent mechanism. These results are very encouraging but further experiments would be necessary to confirm the pharmacological effect of this strategy based on this type of nanoparticles in an in vivo mammalian model.

Declarations

References

1. Johnson IS. Human insulin from recombinant DNA technology. Science. 1983;219:632–7.

2. Usmani SS, Bedi G, Samuel JS, Singh S, Kalra S, Kumar P, Ahuja AA, Sharma M, Gautam A, Raghava GPS. THPdb: Database of FDA-approved peptide and protein therapeutics. PLoS ONE. 2017;12(7):e0181748. https://doi.org/10.1371/journal.pone.0181748.

3. Lau JL, Dunn MK. Therapeutic peptides: Historical perspectives, current development trends, and future directions. Bioorg Med Chem. 2018;26(10):2700–7. https://doi.org/10.1016/j.bmc.2017.06.052.

4. Peptide Therapeutics Market: Global Industry Analysis, Size, Share, Growth, Trends and Forecast 2019–2027 [Internet]. Transpar Mark Res. 2020. Available from: https://www.transparencymarketresearch.com/peptide-therapeutics-market.html

5. Fosgerau K, Hoffmann T. Peptide therapeutics: current status and future directions. Drug Discov Today. 2015;20(1):122–8. https://doi.org/10.1016/j.drudis.2014.10.003.

6. Baig MH, Ahmad K, Saeed M, Alharbi AM, Barreto GE, Ashraf GM, Choi I. Biomed Pharmacother. 2018;103:574–81. https://doi.org/10.1016/j.biopha.2018.04.025.

7. Chauhan NS, Chauhan Nitesh S, Sanjeev C, Vandana H, Alka A, Vijender S. Recent Advances in Insulin Delivery Systems: An Update. World Appl Sci J. 2010;11:1552–6.

8. Khafagy ES, Morishita M, Onuki Y, Takayama K. Current challenges in non-invasive insulin delivery systems: a comparative review. Adv Drug Deliv Rev. 2007;59(15):1521–46. https://doi.org/10.1016/j.addr.2007.08.019.

9. Tracy JA, Dyck PJB. The spectrum of diabetic neuropathies. Phys Med Rehabil Clin N Am. 2008;19(1):1–26. https://doi.org/10.1016/j.pmr.2007.10.010.

10. Ensign LM, Cone R, Hanes J. Oral drug delivery with polymeric nanoparticles: The gastrointestinal mucus barriers. Adv Drug Deliv Rev. 2012;64(6):557–70. https://doi.org/10.1016/j.addr.2011.12.009.

11. Bruno BJ, Miller GD, Lim CS. Basics and recent advances in peptide and protein drug delivery. Ther Deliv. 2013;4(11):1443–67. https://doi.org/10.4155/tde.13.104.

12. Pawar VK, Meher JG, Singh Y, Chaurasia M, Surendar Reddy B, Chourasia MK. Targeting of gastrointestinal tract for amended delivery of protein/peptide therapeutics: Strategies and industrial perspectives. J Control Release. 2014;196:168–83. https://doi.org/10.1016/j.jconrel.2014.09.031.

13. Li YP, Pei YY, Zhang XY, Gu ZH, Zhou ZH, Yuan W-F, Zhou J, Zhu J, Gao X. PEGylated PLGA nanoparticles as protein carriers: synthesis, preparation and biodistribution in rats. J Control Release. 2001;71(2):203–11. https://doi.org/10.1016/s0168-3659(01)00218-8.

14. Inchaurraga L, Martín-Arbella N, Zabaleta V, Quincoces G, Peñuelas I, Irache JM. In vivo study of the mucus-permeating properties of PEG-coated nanoparticles following oral administration. Eur J Pharm Biopharm. 2015;97(Pt A):280–9. https://doi.org/10.1016/j.ejpb.2014.12.021.

15. Schneider CS, Xu Q, Boylan NJ, Chisholm J, Tang BC, Schuster BS, Henning A, Ensign LM, Lee E, Adstamongkonkul P, Simons BW, Wang S-YS, Gong X, Yu T, Boyle MP, Suk JS, Hanes J. Nanoparticles that do not adhere to mucus provide uniform and long-lasting drug delivery to airways following inhalation. Sci Adv. 2017;3(4):e1601556. https://doi.org/10.1126/sciadv.1601556.

16. Martínez-López AL, Pangua C, Reboredo C, Campión R, Morales-Gracia J, Irache JM. Protein-based nanoparticles for drug delivery purposes. Int J Pharm. 2020;581:119289. https://doi.org/10.1016/j.ijpharm.2020.119289.

17. Peñalva R, Esparza I, González-Navarro CJ, Quincoces G, Peñuelas I, Irache JM. Zein nanoparticles for oral folic acid delivery. J Drug Deliv Sci Technol. 2015;30:450–7.

18. Inchaurraga L, Martínez-López AL, Martin-Arbella N, Irache JM. Zein-based nanoparticles for the oral delivery of insulin. Drug Deliv Transl Res. 2020;10(6):1601–11. https://doi.org/10.1007/s13346-020-00796-3.

19. Ruiz-Gatón L, Espuelas S, Huarte J, Larrañeta E, Martin-Arbella N, Irache JM. Nanoparticles from Gantrez® AN-poly(ethylene glycol) conjugates as carriers for oral delivery of docetaxel. Int J Pharm. 2019;571:118699. https://doi.org/10.1016/j.ijpharm.2019.118699.

20. Doktorovova S, Shegokar R, Martins-Lopes P, Silva AM, Lopes CM, Müller RH, Souto EB. Modified Rose Bengal assay for surface hydrophobicity evaluation of cationic solid lipid nanoparticles (cSLN). Eur J Pharm Sci Elsevier. 2012;45(5):606–12. https://doi.org/10.1016/j.ejps.2011.12.016.

21. Abdulkarim M, Agulló N, Cattoz B, Griffiths P, Bernkop-Schnürch A, Borros SG, Gumbleton M. Nanoparticle diffusion within intestinal mucus: Three-dimensional response analysis dissecting the impact of particle surface charge, size and heterogeneity across polyelectrolyte, pegylated and viral particles. Eur J Pharm Biopharm. 2015;97:230–8. https://doi.org/10.1016/j.ejpb.2015.01.023.

22. Inchaurraga L, Martínez-López AL, Cattoz B, Gri PC, Wilcox M, Pearson P, Quincoces G, Peñuelas I, Martin-Arbella N, Irache JM. The effect of thiamine-coating nanoparticles on their biodistribution and fate following oral administration. Eur J Pharm Sci. 2019;128:81–90. https://doi.org/10.1016/j.ejps.2018.11.025.

23. Schindelin J, Arganda-Carreras I, Frise E, Kaynig V, Longair M, Pietzsch T, Stephan Preibisch S, Rueden C, Saalfeld S, Schmid B, Tinevez JY, White DJ, Hartenstein V, Eliceiri K, Tomancak P, Cardona A. Fiji: An open-source platform for biological-image analysis. Nat Methods. 2012;9(7):676–82. https://doi.org/10.1038/nmeth.2019.

24. Brenner S. The genetics of *Caenorabditis elegans*. Genetics. 1974;77(1):71–94.

25. Navarro-Herrera D, Aranaz P, Eder-Azanza L, Zabala M, Hurtado C, Romo-Hualde A, Martínez JA, González-Navarro CJ, Vizmanos JL. Dihomo-gamma-linolenic acid induces fat loss in: *C. elegans* in an omega-3-independent manner by promoting peroxisomal fatty acid β-oxidation. Food Funct. 2018;9(3):1621–1637. https://doi.org/10.1039/c7fo01625e.

26. You Y, Kim J, Raizen DM, Avery L. Insulin, cGMP, and TGF-beta signals regulate food intake and quiescence in *C. elegans*: a model for satiety. Cell Metab. 2008;7(3):249–57. https://doi.org/10.1016/j.cmet.2008.01.005.27.

27. Shen P, Yue Y, Sun Q, Kasireddy N, Kim KH, Park Y. Piceatannol extends the lifespan of *Caenorhabditis elegans* via DAF-16. BioFactors. 2017;43(3):379–87. https://doi.org/10.1002/biof.1346.

28. Yu T, Wang Y, Yang M, Schneider C, Zhong W, Pulicare S, Choi WJ, Mert O, Fu J, Lai SK, Hanes J. Biodegradable mucus-penetrating nanoparticles composed of diblock copolymers of polyethylene glycol and poly(lactic- co -glycolic acid). Drug Deliv Transl Res. 2012;2(2) https://doi.org/10.1007/s13346-011-0048-9.

29. Bajka BH, Rigby NM, Cross KL, Macierzanka A, Mackie AR. The influence of small intestinal mucus structure on particle transport ex vivo. Colloids Surf B Biointerfaces. 2015;135:73–80. https://doi.org/10.1016/j.colsurfb.2015.07.038.

30. Xu Q, Ensign LM, Boylan NJ, Schon A, Gong X, Yang JC, Lamb NW, Cai S, Yu T, Freire E, Hanes J. Impact of surface polyethylene glycol (PEG) density on biodegradable nanoparticle transport in mucus ex vivo and distribution in vivo. ACS Nano. 2015;9(9):9217–27. https://doi.org/10.1021/acsnano.5b038762015;9:9217-27.

31. Lee SJ, Murphy CT, Kenyon C. Glucose shortens the life span of *C. elegans* by Downregulating DAF-16/FOXO Activity and Aquaporin Gene Expression. Cell Metab. 2009;10(5):379–91. https://doi.org/10.1016/j.cmet.2009.10.003.

32. Lu Z, Qiu Z. High glucose concentration restricts fat consumption in *Caenorhabditis elegans*. Int J Clin Exp Med. 2017;10:10554–9.

33. Schlotterer A, Kukudov G, Bozorgmehr F, Hutter H, Du X, Oikonomou D, Ibrahim Y, Pfisterer F, Rabbani N, Thornalley P, Sayed A, Fleming T, Humpert P, Schwenger V, Zeier M, Hamann A, Stern D, Brownlee M, Bierhaus A, Nawroth P, Morcos MC. *elegans* as model for the study of high glucose-mediated life span reduction. Diabetes. 2009;58(11):2450–6. https://doi.org/10.2337/db09-0567.

34. Schulz TJ, Zarse K, Voigt A, Urban N, Birringer M, Ristow M. Glucose restriction extends *Caenorhabditis elegans* life span by Inducing mitochondrial respiration and increasing oxidative stress. Cell Metab. 2007;6(4):280–93. https://doi.org/10.1016/j.cmet.2007.08.011.

35. Zhu G, Yin F, Wang L, Wei W, Jiang L, Qin J. Modeling type 2 diabetes-like hyperglycemia in *C. elegans* on a microdevice. Integr Biol (Camb). 2016;8(1):30–8. https://doi.org/10.1039/c5ib00243e.

36. Yen K, Le TT, Bansal A, Narasimhan SD, Cheng J, Heidi A. A Comparative Study of Fat Storage Quantitation in Nematode *Caenorhabditis elegans* Using Label and Label-Free Methods. PLoS ONE. 2010;5(9):e12810. https://doi.org/10.1371/journal.pone.0012810.

37. Nomura T, Horikawa M, Shimamura S, Hashimoto T, Sakamoto K. Fat accumulation in *Caenorhabditis elegans* is mediated by SREBP homolog SBP-1. Genes Nutr. 2010;5(1):17–27. https://doi.org/10.1007/s12263-009-0157-y.

38. Garcia AM, Ladage ML, Dumesnil DR, Zaman K, Shulaev V, Azad RK, et al. Glucose induces sensitivity to oxygen deprivation and modulates Insulin/IGF-1 signaling and lipid biosynthesis in *Caenorhabditis elegans*. Genetics. 2015;200(1):167–84. https://doi.org/10.1534/genetics.115.174631.

39. Mendler M, Schlotterer A, Ibrahim Y, Kukudov G, Fleming T, Bierhaus A, Padilla PA. daf-16/FOXO and glod-4/glyoxalase-1 are required for the life-prolonging effect of human insulin under high glucose conditions in *Caenorhabditis elegans*. Diabetologia. 2014;58:393–401.

40. Dimov I, Maduro MF. The *C. elegans* intestine: organogenesis, digestion, and physiology. Cell Tissue Res. 2019 Sep;377(3):383–96. https://doi.org/10.1007/s00441-019-03036-4.

41. Everman JL, Ziaie NR, Bechler J, Bermudez LE. Establishing *Caenorhabditis elegans* as a model for *Mycobacterium avium* s*ubspecies hominissuis* infection and intestinal colonization. Biol Open. 2015;4(10):1330–5. https://doi.org/10.1242/bio.012260.